ARTICLES
PUBLISHED ONLINE: 20 JULY 2014 | DOI: 10.1038/NNANO.2014.140

nature nanotechnology

Optical trapping of individual human immunodeficiency viruses in culture fluid reveals heterogeneity with single-molecule resolution

Yuanjie Pang, Hanna Song, Jin H. Kim, Ximiao Hou† and Wei Cheng*

Optical tweezers use the momentum of photons to trap and manipulate microscopic objects, contact-free, in three dimensions. Although this technique has been widely used in biology and nanotechnology to study molecular motors, biopolymers and nanostructures, its application to study viruses has been very limited, largely due to their small size. Here, using optical tweezers that can simultaneously resolve two-photon fluorescence at the single-molecule level, we show that individual HIV-1 viruses can be optically trapped and manipulated, allowing multi-parameter analysis of single virions in culture fluid under native conditions. We show that individual HIV-1 differs in the numbers of envelope glycoproteins by more than one order of magnitude, which implies substantial heterogeneity of these virions in transmission and infection at the single-particle level. Analogous to flow cytometry for cells, this fluid-based technique may allow ultrasensitive detection, multi-parameter analysis and sorting of viruses and other nanoparticles in biological fluid with single-molecule resolution.

Optical tweezers[1–5] have been widely used to study molecular motors and biopolymers[3,6–15], and for trapping of metal nanoparticles[16–18] and various nanostructures[4,19–22]. However, there have been no demonstrations or studies on optical manipulation of a single animal virus[23]. Several challenges exist besides the issue of biosafety. First, the presence of a permanent or an induced dipole moment in the object is required for optical trapping[3]. Ashkin and Dziedzic first demonstrated optical trapping of tobacco mosaic virus (TMV) in 1987[23]. TMV is 300 nm long and 15 nm in diameter[24]. This long cylindrical structure has a permanent dipole moment[25] that may facilitate its trapping by optical tweezers. The majority of animal viruses are spherical[26,27], and their dipole moments may be intrinsically small compared with other aspheric objects of similar volume[23]. Second, animal viruses are typically less than 300 nm in size[26,27]. The gradient force responsible for the trapping of a Rayleigh scatterer scales with the cube of the particle dimension[3]. The lower viscous drag from the solvent on smaller particles also allows them to escape easily once trapped. Hence, the smaller the particle, the more difficult it is to trap and manipulate it using light. Third, the refractive indices of animal viruses have never been measured. Although, in general, the trapping force increases with the refractive index of the object[28], how a single animal virus may interact with light rays and generate trapping forces on itself is unknown. All these aspects present challenges to the manipulation of an animal virus using light. Indeed, can a single animal virus be trapped and manipulated using light? Here, by using an ultrahigh-resolution optical tweezers instrument that we constructed recently[29], we show that individual human immunodeficiency virus type 1 (HIV-1) can be trapped and manipulated in culture fluid—contact-free—in three dimensions under native conditions. We have developed this capability into a quantitative technique, named as 'virometry'. This technique permits multi-parameter analysis of individual HIV-1 virions in culture fluid under native conditions with single-molecule resolution, and can be applied to other viruses and nanoparticles in solution for their detection and the measurement of size, shape and protein compositions with unprecedented sensitivity.

Optical trapping of single HIV-1 in culture fluid

To demonstrate the optical trapping of animal viruses in biological fluid, we have recently prepared HIV-1 virions derived from the X4-tropic NL4-3 provirus clone[30]. These viruses were tagged internally with enhanced green fluorescent protein (EGFP) fused to Vpr[31,32], an accessory protein of HIV that physically associates with the virion core[33] and thus serves as a fluorescent marker[31] for virion manipulation. The infectivity of this virus was 0.1% in TZM-bl cells[30], a value that is comparable to that for wild-type viruses. Control experiments showed that EGFP–Vpr also distinguishes virions from microvesicles (Supplementary Section 1). Without any fixation procedure, we diluted the live virus stock in the complete media and injected them into a microfluidic chamber (Fig. 1a). Upon trapping of a virion by the 830 nm infrared laser[29], focused at the centre of the chamber, the virion was immediately 'visible' in the dark background due to simultaneous two-photon excitation of EGFP by the trapping laser[29,34] (Fig. 1b). Such events were not observed when complete media only, viruses without EGFP–Vpr labels, or culture supernatants transfected with EGFP–Vpr were used as controls, suggesting that the fluorescent particles resulted from virions tagged with EGFP. Under these conditions, a single fluorescent particle could be trapped in culture fluid and manipulated in various patterns by steering the laser beam without interference from other virions (Supplementary Movie). Typical two-photon fluorescence (TPF) time courses from individually trapped virions are presented in Fig. 1c, where the initial bursts of fluorescence well above background indicate the arrival of HIV-1 virions at the optical trap. The subsequent decay of TPF with time could all be fit by single exponentials with an average time constant of 53.7 ± 8.0 s ($N = 19$), very close to the rate of photobleaching that we measured previously for EGFP either on a surface (50.8 ± 4.2 s)[34] or inside a cell (52.7 ± 5.2 s)[35]. This comparison confirms the presence of EGFP in these particles.

Department of Pharmaceutical Sciences, University of Michigan, 428 Church Street, Ann Arbor, Michigan 48109, USA; †Present address: College of Life Sciences, Northwest A&F University, Shaanxi, China. *e-mail: chengwe@umich.edu

© 2014 Macmillan Publishers Limited. All rights reserved.

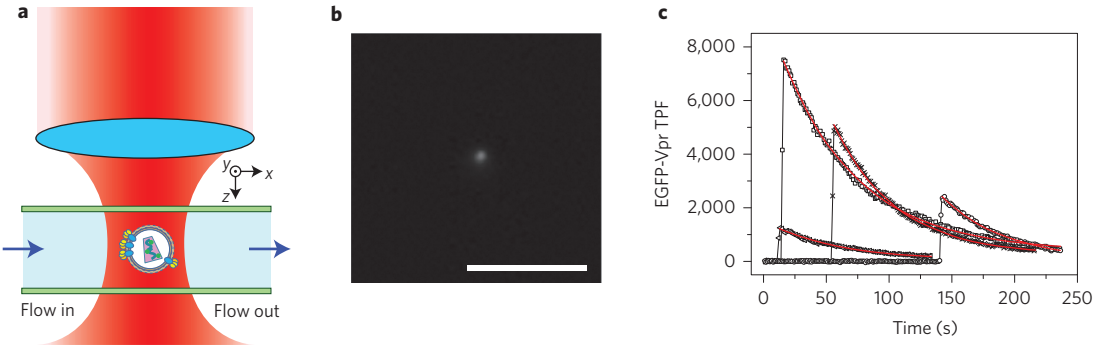

Figure 1 | Optical trapping of HIV virions in culture fluid. a, HIV-1 virions are delivered into a microfluidic chamber and trapped by an infrared laser focused at the centre of the chamber. The *xyz* dimensions are indicated, with *y* perpendicular to the figure plane. **b**, Two-photon fluorescence (TPF) image of a trapped HIV virion. Scale bar, 10 μm. **c**, Representative TPF time courses from individually trapped HIV virions. All traces are fit with single exponential decay (red), with time constants for each trace as follows: 60.7 s (squares), 49.5 s (crosses), 51.5 s (circles) and 54.1 s (triangles). Time zero represents the onset of TPF collection.

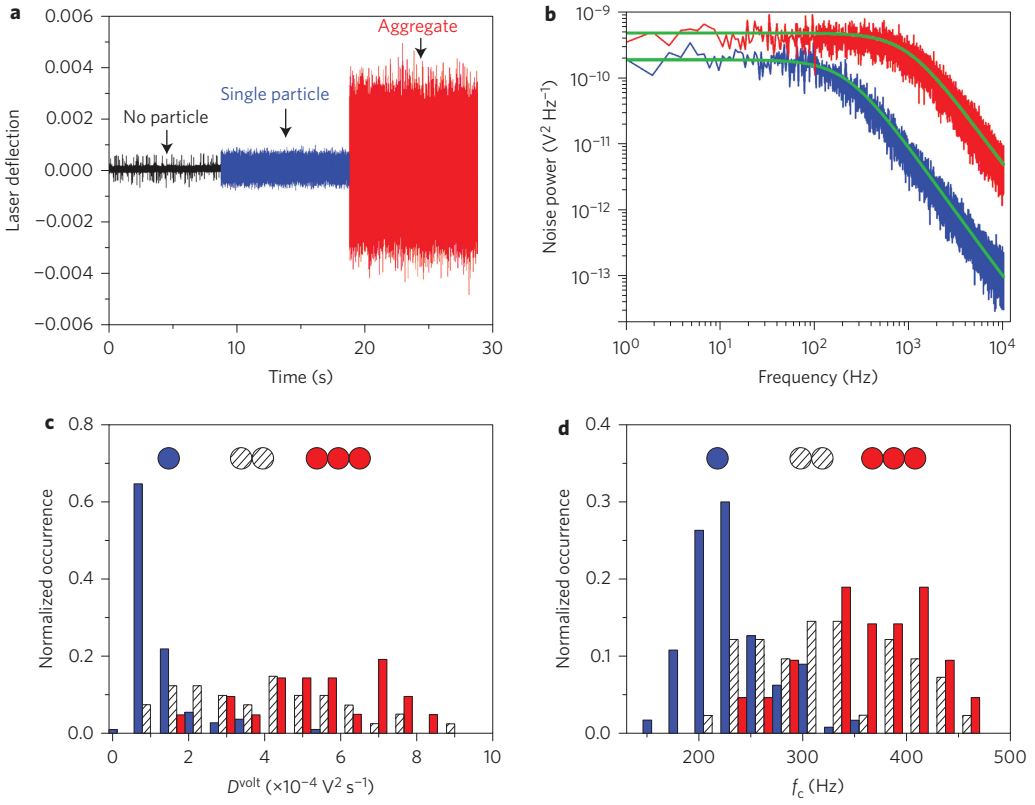

Figure 2 | Back focal plane interferometry to distinguish a single HIV-1 particle from aggregates in complete media. a, Laser deflection signal measured in real time using back focal plane (BFP) interferometry. **b**, Power spectra calculated from the data shown in **a** and fits (green curves) to an aliased Lorentzian with $D^{volt} = 8.53 \times 10^{-5}$ V^2 s^{-1}, $f_c = 223$ Hz (blue) and $D^{volt} = 0.0046$ V^2 s^{-1}, $f_c = 982$ Hz (red). **c**,**d**, Histograms for D^{volt} (**c**) and f_c (**d**), derived from Lorentzian fitting parameters for apparent one (blue, $N = 110$), two (hashed, $N = 41$) and three (red, $N = 21$) particles trapped, with cartoons representing one, two and three particles above the histograms.

Freely diffusing particles in culture fluid may undergo concentration-dependent aggregation. How do we know that the trapped particle corresponds to a single HIV-1 virion? Independent of EGFP fluorescence, we could also detect the trapping of the virus from changes in laser deflection at the objective's back focal plane (BFP) (Fig. 2a, blue). The occasional trapping of an apparent viral aggregate produced quantitatively different laser deflection signals[29,36] (Fig. 2a, red), suggesting that one could potentially use this signal to distinguish viral particles of different size. We analysed the time courses of the laser deflection by conversion to power spectra in the frequency domain (Fig. 2b). For both the single particle (blue) and virion aggregate (red), the power spectra could be well described with a Lorentzian up to 10 kHz (green curves; Supplementary Methods), consistent with the Brownian motion of a particle in a harmonic photonic field[3]. Furthermore, this fitting yielded very different values of D^{volt} (the diffusion coefficient, in V^2 s^{-1}) and f_c (the corner frequency, in Hz) for the single particle and virion aggregate. To test the sensitivity of these parameters in differentiating particles of different size, we delivered diluted virions through a microfluidic channel into the complete

© 2014 Macmillan Publishers Limited. All rights reserved.

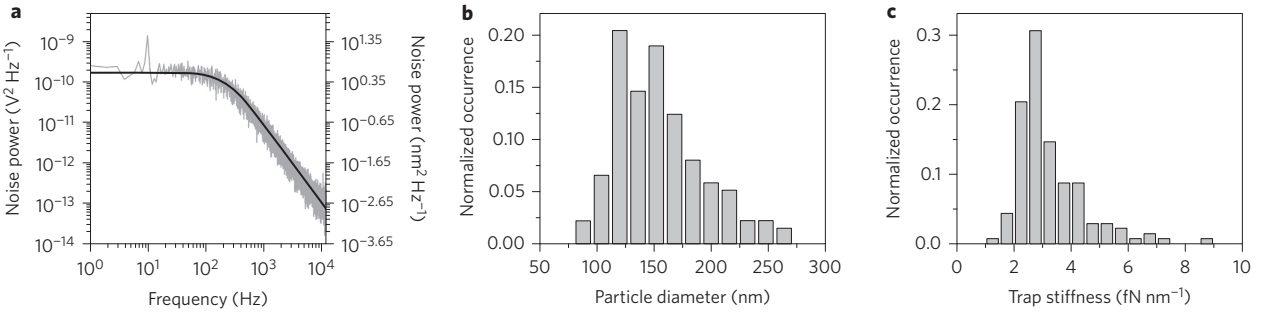

Figure 3 | Measurement of diameter for single HIV-1. a, Power spectrum of a trapped virion when the chamber is oscillated at 10 Hz with an amplitude of 176 nm along the *y* axis of the sample plane (see Methods). Black curve: fit of the thermal noise background to the aliased Lorentzian with $D^{volt} = 9.37 \times 10^{-5}$ V^2 s^{-1} and $f_c = 233$ Hz. **b**, Size histogram for single fluorescent particles from chamber oscillation along the *y* axis ($N = 137$). The concentration of HIV-1 inside the chamber is 4.0×10^7 virions ml^{-1}. **c**, Distribution of optical trap stiffness for each virion trapped ($N = 137$).

media, followed by trapping of the virion in the vicinity of the channel opening (Supplementary Fig. 1). This scheme allowed us to trap one, two and three particles sequentially using a single laser beam (Supplementary Fig. 1), and measure D^{volt} and f_c for the apparent single, double and triple particles, respectively. The distributions of these values are plotted in Fig. 2c and d, respectively. As shown, both D^{volt} and f_c conform to statistically different distributions for single versus double or triple particles (Supplementary Table 1), suggesting that the laser deflection is sensitive enough to distinguish a single particle from particle aggregates.

Measurement of single HIV-1 virion diameter

Single HIV-1 particles are heterogeneous in diameter[37]. To help distinguish individual viral particles with different diameters, we set out to use the sensitive laser deflection signal to directly measure the diameter for each trapped virion in the culture fluid (see Methods). This method works by calibration of the laser deflection signal using a distance standard[38], and D^{volt} can be converted to the diffusion coefficient of the particle in space (D, in μm^2 s^{-1})[38]. The diameter of the particle, ϕ_{BFP}, can then be calculated using the Stokes–Einstein equation (Supplementary Methods). We first tested this method by trapping polystyrene beads of various sizes in water. These results were compared with the diameters of the beads determined from transmission electron microscopy (TEM) images (ϕ_{TEM}, Supplementary Fig. 2). Over the range of bead sizes we tested, these two methods yielded good agreement, with ϕ_{BFP} slightly larger than ϕ_{TEM} by 5.5% on average, which reflected either the error in laser deflection measurement or hydration of particles in water. Figure 3a presents the power spectrum of a trapped virion obtained from this calibration procedure in complete media, with voltage converted to distance as shown on the right axis, which yields a diameter of 165 nm for this particular virion. Figure 3b shows the histogram of ϕ_{BFP} determined for 137 single HIV-1 particles in complete media at a concentration of 4.0×10^7 virion ml^{-1}, which shows a population with a mean of 154 nm, and a median of 148 nm. The reduced chi-squared statistic from this analysis varies from 1.10 to 1.16 (Supplementary Fig. 3), indicating a good quality of power spectrum fitting. This virion size distribution is quantitatively similar to that reported previously for authentic, mature HIV-1 virions by cryoelectron microscopy (cEM)[37]. Our mean diameter is 6.2% larger than the 145 ± 25 nm measured for single HIV virions using cEM. This positive deviation is consistent with the trend seen for reference beads, suggesting that these particles indeed correspond to single virions in complete media. This positive deviation can result from either hydration of the particles in culture media or potential shrinkage of the feature size under electron microscopy (Supplementary Section 2). From the calibrated power spectra for single HIV-1 virions, we also obtain the stiffness of the optical trap (Supplementary Methods), which is shown in Fig. 3c to have a mean value of 3.2 fN nm^{-1}. This stiffness is about 30-fold lower than typically reported values for bigger particles[3] and explains the difficulty in trapping virions of this size. The variation in trap stiffness compared to variations in particle diameter also suggests that HIV-1 virions deviate from true Rayleigh scatterers. To examine how well the measured particle diameter and trap stiffness can differentiate particles of different size, we conducted sequential trapping of one, two and three particles, as shown in Supplementary Fig. 1, and measured ϕ_{BFP} and trap stiffness for the apparent single, double and triple particles, respectively. The distributions of these values are plotted in Supplementary Fig. 4a,b. As shown, both ϕ_{BFP} and trap stiffness conform to statistically different distributions for single versus double or triple particles (Supplementary Table 2), suggesting that these parameters are sensitive enough to distinguish a single particle from particle aggregates.

Concentration-dependent aggregation of HIV-1 virions

Freely diffusing particles in the complete media may undergo concentration-dependent aggregation. To examine the aggregation status of HIV-1 virions under native conditions in complete media, we conducted diameter measurement for single particles trapped at various concentrations in the microfluidic chamber. Figure 4a presents a histogram of ϕ_{BFP} determined for 128 apparent single particles at 1.2×10^8 virions ml^{-1} in complete media (grey bars), showing two distinct populations, as indicated by the double-Gaussian fit (dashed lines). The primary peak, with a mean of 156 nm and a standard deviation of 30 nm, accounts for 72% of the particles. This number is very close to the average diameter of 154 nm for single HIV virions measured at 4.0×10^7 virions ml^{-1}, suggesting that these particles indeed correspond to single virions. The secondary peak in this histogram, with a mean of 305 nm and a standard deviation of 44 nm, is about twice as large as a typical HIV-1 virion. These particles were rarely observed when trapping at a concentration of 4.0×10^7 virions ml^{-1}, suggesting that they resulted from a concentration-dependent aggregation. This conclusion is further supported by the same experiment carried out at an even higher concentration of virion particles. Figure 4b shows the histogram of ϕ_{BFP} determined for 103 apparent single particles at 4.0×10^8 virions ml^{-1} in complete media. No clear peaks are present. The particle diameters range from 90 to 440 nm, with an average diameter of 232 ± 78 nm (median of 219 nm). This feature is reproducible from an independent repeat of the same experiment, suggesting a concentration-dependent aggregation of HIV-1 particles. Figure 4c shows the distribution of EGFP TPF intensity from single HIV-1 virions upon their initial trapping. This distribution was broad and asymmetric, ranging from 1,000 to 40,000 a.u., with a major peak around 30,000. This variation of

© 2014 Macmillan Publishers Limited. All rights reserved.

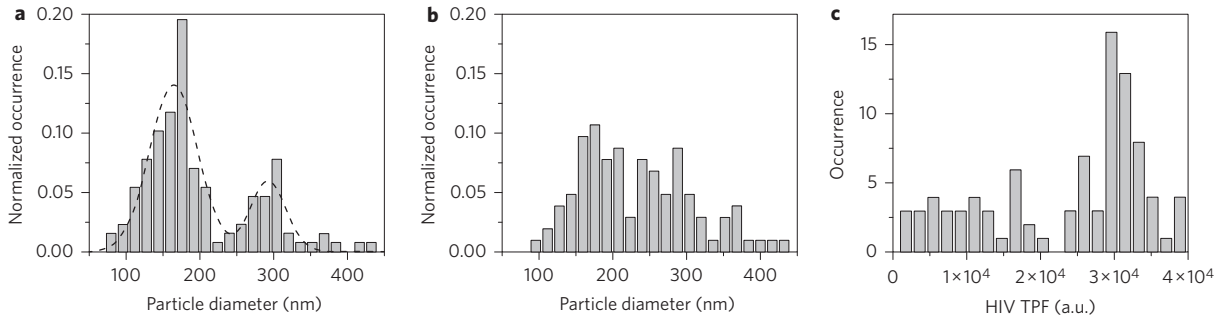

Figure 4 | Aggregation of HIV-1 observed at high virion concentrations. a, Size histogram for single fluorescent particles from chamber oscillation along the *y* axis and its double-Gaussian fit (dashed line; $N = 128$). The concentration of HIV-1 inside the chamber is 1.2×10^8 virions ml^{-1}. **b**, Size histogram for single fluorescent particles from chamber oscillation along the *y* axis ($N = 103$). The concentration of HIV-1 inside the chamber is 4.0×10^8 virions ml^{-1}. **c**, Distribution of EGFP–Vpr two-photon fluorescence (TPF) intensity from trapped virions that are confirmed to be single based on the diameter measurements in **a** ($N = 92$).

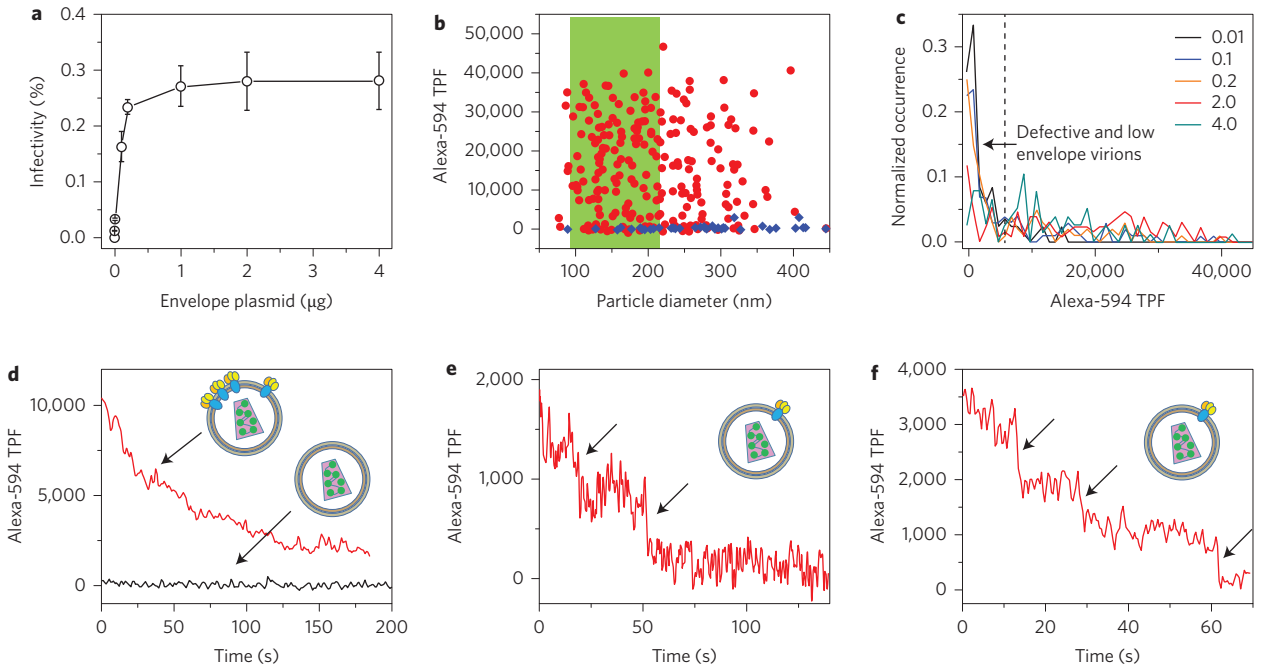

Figure 5 | Optical trapping virometry. a, Infectivity of HIV-1 virions as a function of pEnv in the presence of 20 μg ml^{-1} DEAE–dextran. Error bars are standard deviations from three independent replicates. **b**, Alexa-594 two-photon fluorescence (TPF) as a function of particle diameter. Red circles represent HIV-1 from 2 μg pEnv ($N = 231$) and blue diamonds represent virions without envelopes ($N = 42$). The green shaded area represents diameters between 96 and 216 nm that were consistent with single HIV-1 virions (Supplementary Methods). **c**, TPF intensity histograms for Alexa-594 from single HIV-1 particles, with black, blue, orange, red and olive curves for virions from 0.01 ($N = 84$), 0.1 ($N = 102$), 0.2 ($N = 100$), 2.0 ($N = 128$) and 4.0 μg ($N = 76$) pEnv, respectively. **d–f**, Representative Alexa-594 TPF time courses from single virions bound with Alexa-594–b12, with individual photobleaching steps in **e** and **f** indicated by arrows. Insets: Cartoons of HIV-1 virions with varied numbers of envelope glycoproteins.

TPF intensity exclusively resulted from EGFP–Vpr molecules packaged into virions, because control virions without EGFP showed no detectable TPF under these conditions. This substantial variation of the initial TPF amplitudes suggests that one cannot simply use TPF intensity to confirm a single virus. Rather, size or trap stiffness measurements are required. Moreover, virion diameter is a better parameter than D^{volt} in resolving subpopulations within a virus pool (Supplementary Fig. 5).

Optical trapping virometry

We have recently developed single-molecule TPF imaging capability using our optical trap set-up[34,35]. This imaging uses the optical trapping laser for direct and simultaneous TPF excitation of fluorophores, such as fluorescent proteins at the laser focus, whose fluorescence is detectable at the single-molecule level. Because the optical paths for BFP interferometry operate independently from single-molecule TPF detection, we can thus trap a single HIV-1 in culture fluid and simultaneously monitor viral proteins via TPF by using appropriate fluorophore labels. Because our TPF detection has single-molecule sensitivity, this technique should offer many possibilities for quantitation and potential sorting of virions in culture fluid, with exquisite sensitivity. To test this idea we produced series of HIV-1 virions that were tagged with EGFP–Vpr but might carry a different number of envelope glycoproteins, because we varied the envelope plasmid input (pEnv, 0–4 μg) during virion production[30]. The infectivity of these virions increased with increasing pEnv (Supplementary Fig. 6) and reached a plateau at 1 μg pEnv in the presence of 20 μg ml^{-1} diethylaminoethyl-dextran (DEAE-dextran) (Fig. 5a). To monitor the envelope content of individual virions, we prepared fluorescently labelled monoclonal

© 2014 Macmillan Publishers Limited. All rights reserved.

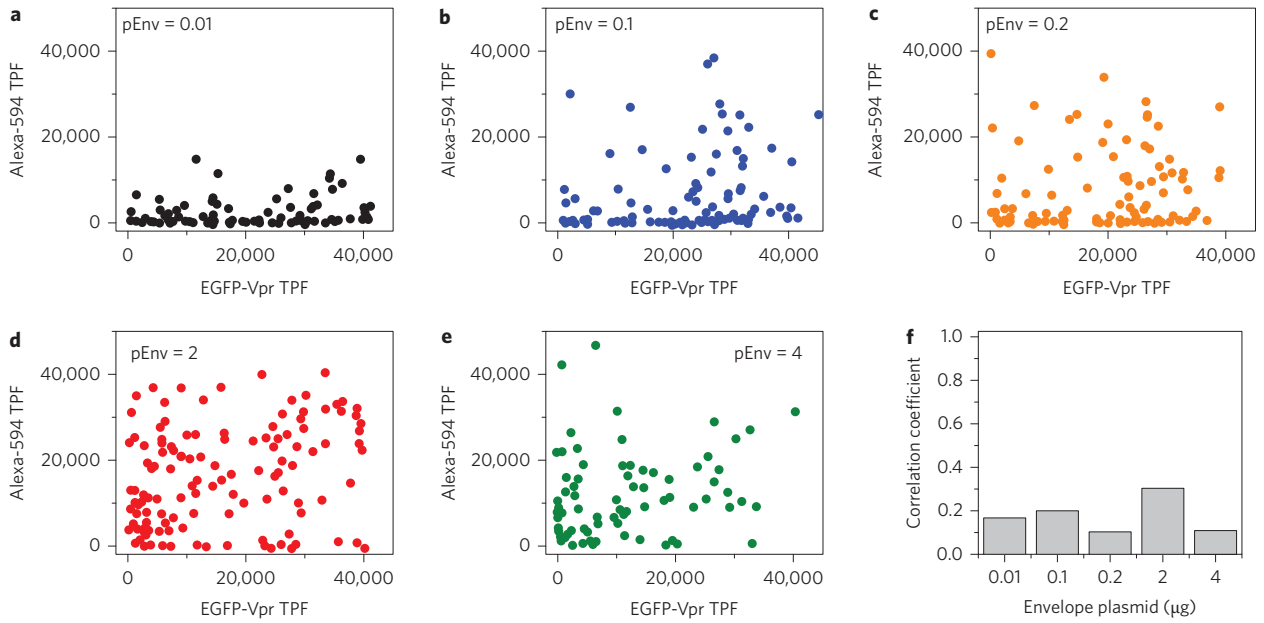

Figure 6 | Two-colour correlation analysis for EGFP–Vpr and envelope glycoproteins in single HIV-1 virions. a–e, Alexa-594 TPF is plotted as a function of EGFP–Vpr TPF for virions prepared with 0.01, 0.1, 0.2, 2 and 4 μg pEnv, as indicated (colour code as in Fig. 5c). **f**, Correlation coefficients calculated for **a–e** as a function of pEnv inputs during virion production.

antibody b12 (ref. 39) (Alexa-594–b12), which specifically recognizes HIV-1 envelope glycoproteins gp120 (refs 40,41). We chose Alexa-594 for labelling, as this can be efficiently excited by the 830 nm trapping laser and yet has a minimal spectral overlap with EGFP emission (Supplementary Fig. 7). This strategy allowed us to measure EGFP–Vpr and gp120 for the same single virion almost simultaneously, both with single-molecule sensitivity[34] (Supplementary Fig. 8). Microvesicles that carried gp120 or antibody aggregates were also excluded from HIV-1 virions by using this two-colour strategy. We incubated the EGFP-tagged viruses with Alexa-594–b12 at an antibody concentration (15 μg ml^{-1}) that was sufficient to neutralize more than 95% HIV infectivity (Supplementary Fig. 9) to ensure the saturation binding of all functional gp120. Control experiments showed that gp120 shedding was negligible at this concentration of b12 (Supplementary Fig. 10). We thus expect the level of Alexa-594–b12 fluorescence associated with individual virions to correlate with gp120 content on the virion surface. We measured HIV virions prepared with 0, 0.01, 0.1, 0.2, 2 and 4 μg pEnv by trapping them in complete media. A typical result is shown in Fig. 5b using 2 μg pEnv as an example, where the intensity of Alexa-594 TPF for each particle is plotted as a function of particle diameter (red circles; $N = 231$). For 2 μg pEnv, 55% of particles had diameters that were consistent with single virions (highlighted in green in Fig. 5b). The intensity of Alexa-594 TPF associated with these particles displayed a broad distribution, varying from zero to 40,000 a.u. Control experiments using virions without envelope glycoproteins (pEnv = 0) showed no Alexa-594 fluorescence in more than 95% of cases (Fig. 5b, blue diamonds), confirming that the different levels of Alexa-594 TPF resulted from specific gp120 binding by Alexa-594–b12. Figure 5c shows a compendium of Alexa-594 TPF histograms from single virions prepared with varied pEnv. Throughout, all the distributions were broad, even when the infectivity for the corresponding batch of HIV-1 was at a plateau. The single-molecule sensitivity of the current set-up allows us to roughly estimate the number of envelope trimers in single virions based on the average TPF intensity of a single Alexa-594 molecule. This yielded 0–18 envelope trimers per virion if we assume that each Alexa-594–b12 binds two gp120 molecules, or 0–9 envelope trimers per virion if each Alexa-594–b12 binds only one gp120 (Supplementary Section 3). Indeed, as shown in Fig. 5d, we could clearly distinguish particles that carried gp120 (red curve) from those that did not because of this single-molecule sensitivity (black curve). Of the single particles from 2 μg pEnv, 12% did not show any Alexa-594 fluorescence (Fig. 5c), indicating that no gp120 was present on the virion surface. This fraction increased to 26% as we lowered the pEnv to 0.01 μg (Fig. 5c). Because envelope glycoproteins are required for virion infectivity (Fig. 5a), these data suggest that defective HIV-1 virions can be produced during virion budding, the fraction of which increases when envelope glycoproteins are supplied under limiting conditions (Supplementary Table 3). Furthermore, there were particles that had gp120 but clearly showed only two or three steps of Alexa-594 photobleaching (Fig. 5e,f). The fraction of these virions was 5% for 2 μg pEnv and increased to 33% for virions prepared with 0.01 μg pEnv. These data indicate that, at most, a single envelope trimer is present on these virions. The number of envelope trimers per virion has been estimated previously using various methods[42,43]. However, estimates as low as a single trimer on a virion surface have not been reliably reported. Our technique allows us to clearly detect the presence of a single trimer on an HIV-1 virion surface in culture fluid, without ambiguity.

Finally, the ability of our technique to use a single 830 nm laser to simultaneously excite both EGFP and Alexa-594 offers a unique advantage. Because EGFP and Alexa-594 have minimal emission spectrum overlap (Supplementary Fig. 7), we can resolve both fluorescences for a single HIV-1 particle and thus examine the potential correlation between the two kinds of proteins within a single particle. To this end, we plot Alexa-594 TPF as a function of EGFP–Vpr TPF for each single HIV-1 virion in Fig. 6a–e for the five batches of viruses prepared with different pEnv inputs. As shown, there was little correlation between Alexa-594 and EGFP–Vpr in their TPF intensities at the single-particle level. This conclusion is true regardless of the input quantity of pEnv. The correlation coefficients between Alexa-594 TPF and EGFP–Vpr TPF are 0.1668, 0.2002, 0.1035, 0.3054 and 0.1087 for 0.01, 0.1, 0.2, 2 and 4 μg

© 2014 Macmillan Publishers Limited. All rights reserved.

pEnv (Fig. 6f), respectively, suggesting that Vpr and envelope glycoprotein incorporation into individual HIV-1 virions are two independent processes during HIV-1 virion budding.

Optical trapping of a single animal virus

The optical trapping technique has been widely used in biology and nanotechnology to study molecular motors, biopolymers and various nanostructures. However, there have been no demonstrations or studies on the optical manipulation of any animal virus, largely due to the small size of these particles. Here, we show that it is feasible to optically manipulate a single HIV-1 virion in culture fluid. Our technique combines sensitive BFP interferometry[36,44] and simultaneous TPF at the single-molecule level in a single experimental set-up, allowing multi-parameter analysis of a single HIV-1 virion in culture fluid with single-molecule resolution (Supplementary Section 4). Analogous to flow cytometry for cells, this technique may well be applied to a broad spectrum of animal viruses[26] for ultrasensitive detection, multi-parameter analysis of particle heterogeneity, and potential sorting in biological fluid.

Heterogeneity of HIV-1 virions

Much is known about the heterogeneity of RNA viruses at the nucleic acid level thanks to advances in DNA sequencing technology. However, little is known about the heterogeneity of RNA viruses in their protein compositions because of a lack of sensitive techniques to measure viral protein contents at the single-molecule level per virion basis. Virometry directly reveals the heterogeneity of HIV-1 in terms of protein composition with single-molecule sensitivity. For gp120, we found that its copy number varied over one order of magnitude, despite the fact that all these virions were derived from a single clone. This property is a feature of single HIV-1 virions, as demonstrated by our analysis using different cutoff values for single virion diameters (Supplementary Fig. 11). The consequence of this variation might be a broad spectrum of infectivity for individual HIV-1 virions, as shown in Fig. 5a and hypothesized in the literature[45]. Indeed, recent studies have shown that the transmitted 'founder' virus that establishes infection in AIDS patients corresponds to virions with a higher envelope glycoprotein content[46]. Future experiments are necessary to determine if the heterogeneity observed in the spike number of NL4-3 virions is also relevant to R5-tropic viruses, which are generally believed to establish primary infections[47]. The substantial heterogeneity of envelope content in virions from both low and high pEnv inputs indicates a stochastic component in envelope glycoprotein incorporation during virion budding[48–50]. It will be of interest in the future to dissect the mechanisms behind this apparent heterogeneity in viral envelope content, whether it results from a passive incorporation process or an active recruitment mechanism through protein–protein interactions[48,49,51].

Methods

Production of HIV-1 virions. Various HIV-1 virions were generated and assayed as described recently[30]. Briefly, 293T cells were transfected with 1.0 μg pNL4-3R$^-$E$^-$ plasmid, various amounts of pEnv (NL4-3 envelope expression plasmid, the same as pcDNA3.1REC in ref. 30) and pEGFP–Vpr using Mirus LT-1 transfection reagents in 2 ml culture volume in a 35 mm dish. pEnv (0.1 μg) and 0.3 μg pEGFP–Vpr plasmids were used as default unless otherwise noted. The medium was changed 6 h post-transfection, and virions were harvested at 24 h post-transfection[30]. Infectious virion concentrations were measured using the TZM-bl indicator cell line, and the physical concentrations of virion particles were determined using a p24 enzyme-linked immunosorbent assay (ELISA) as previously described[30]. The infectivity of the virions was calculated by taking the ratio between infectious virion concentration and physical particle concentration. More than 90% of the infectious units were retained in the complete media over the timeframe of the experiments (Supplementary Fig. 12).

OTs and TPF experiments. A home-made optical tweezers instrument using a tapered amplifier diode laser at 830 nm (SYS-420-830-1000, Sacher LaserTechnik LLC) was used for optical trapping and simultaneous TPF measurement of HIV-1 virions[29]. Briefly, the trapping laser was focused to a diffraction limited spot using a ×60 water-immersion microscope objective (Nikon) with a numerical aperture of 1.2. We diluted the live virus stock in complete media to a concentration of ~0.4–4.0 × 10^8 virions ml^{-1} and injected them into a microfluidic chamber for optical trapping. Brownian motion of the trapped virions was recorded using BFP interferometry[44] at 62.5 kHz for 10 s (ref. 36). To measure the virion diameter in culture fluid, a closed-loop nanopositioning stage (3D200, Mad City Labs) was used to oscillate the microfluidic chamber, the amplitude of which was measured directly using video microscopy (Supplementary Fig. 13). For trapping of virions, control experiments showed that oscillation did not induce any change in the thermal background. An electron-multiplying charge-coupled device (EMCCD) camera (Evolve, Photometrics) was used for all fluorescence detection. To collect TPF with single-molecule sensitivity, a motorized filter wheel was installed in front of the EMCCD camera, in which the TPF from EGFP was monitored using an emission filter HQ525/50m (Chroma) and Alexa-594 was monitored using emission filter ET645/75 (Chroma). In addition, a short-pass filter (E700sp-2p, Chroma) was installed in front of the EMCCD camera to block the 830 nm trapping laser. A laser power of 130.8 mW at the focus was used throughout for optical trapping and simultaneous TPF excitation. The laser power was monitored using a position-sensitive detector and kept within 1% variation throughout all experiments. The fluorescence averaged over the initial 2 s exposure time was recorded as the initial fluorescence of the virion. For the two-colour experiments, the viruses bound with Alexa-594–b12 were injected into the microfluidic chamber. Upon trapping of individual particles in culture media, the TPF emission from Alexa-594 was measured first and the filter then switched to the EGFP channel to measure EGFP TPF. The residue leakage of EGFP channel fluorescence into the Alexa-594 channel was experimentally measured and quantified by linear regression (Supplementary Fig. 7), and this information was used to correct for Alexa-594 TPF throughout. All TPF data were collected as described using a Nis-Element (Nikon), with an electron-multiplication gain of 200 and exposure time of 400 ms, except the TPF time courses in Fig. 1, where an exposure time of 1 s without gain was used. All the trapping and TPF experiments were conducted at a constant temperature of 20.0 ± 0.2 °C in complete media, which consisted of DMEM supplemented with 10% fetal bovine serum (HyClone). The step-finding algorithm that we developed recently[52] was used to identify steps from all single-molecule traces. All the correlation analysis was performed using custom-written MATLAB scripts and the correlation coefficients were calculated using MATLAB built-in functions. Throughout this work, all errors are standard deviations unless otherwise noted.

Received 13 February 2014; accepted 12 June 2014; published online 20 July 2014

References

1. Ashkin, A., Dziedzic, J. M., Bjorkholm, J. E. & Chu, S. Observation of a single-beam gradient force optical trap for dielectric particles. *Opt. Lett.* **11,** 288–290 (1986).
2. Grier, D. G. A revolution in optical manipulation. *Nature* **424,** 810–816 (2003).
3. Neuman, K. C. & Block, S. M. Optical trapping. *Rev. Sci. Instrum.* **75,** 2787–2809 (2004).
4. Marago, O. M., Jones, P. H., Gucciardi, P. G., Volpe, G. & Ferrari, A. C. Optical trapping and manipulation of nanostructures. *Nature Nanotech.* **8,** 807–819 (2013).
5. Qian, B., Montiel, D., Bregulla, A., Cichos, F. & Yang, H. Harnessing thermal fluctuations for purposeful activities: the manipulation of single micro-swimmers by adaptive photon nudging. *Chem. Sci.* **4,** 1420–1429 (2013).
6. Wang, M. D. Manipulation of single molecules in biology. *Curr. Opin. Biotechnol.* **10,** 81–86 (1999).
7. Perkins, T. T., Quake, S. R., Smith, D. E. & Chu, S. Relaxation of a single DNA molecule observed by optical microscopy. *Science* **264,** 822–826 (1994).
8. Heller, I. *et al.* STED nanoscopy combined with optical tweezers reveals protein dynamics on densely covered DNA. *Nature Methods* **10,** 910–916 (2013).
9. Aubin-Tam, M. E., Olivares, A. O., Sauer, R. T., Baker, T. A. & Lang, M. J. Single-molecule protein unfolding and translocation by an ATP-fueled proteolytic machine. *Cell* **145,** 257–267 (2011).
10. Bormuth, V., Varga, V., Howard, J. & Schaffer, E. Protein friction limits diffusive and directed movements of kinesin motors on microtubules. *Science* **325,** 870–873 (2009).
11. Gross, S. P. Application of optical traps *in vivo*. *Methods Enzymol.* **361,** 162–174 (2003).
12. Vale, R. D. Microscopes for fluorimeters: the era of single molecule measurements. *Cell* **135,** 779–785 (2008).
13. Yanagida, T., Iwaki, M. & Ishii, Y. Single molecule measurements and molecular motors. *Phil. Trans. R. Soc. Lond. B* **363,** 2123–2134 (2008).
14. Stigler, J., Ziegler, F., Gieseke, A., Gebhardt, J. C. M. & Rief, M. The complex folding network of single calmodulin molecules. *Science* **334,** 512–516 (2011).
15. Tinoco, I. Jr Force as a useful variable in reactions: unfolding RNA. *Annu. Rev. Biophys. Biomol. Struct.* **33,** 363–385 (2004).
16. Bosanac, L., Aabo, T., Bendix, P. M. & Oddershede, L. B. Efficient optical trapping and visualization of silver nanoparticles. *Nano Lett.* **8,** 1486–1491 (2008).

© 2014 Macmillan Publishers Limited. All rights reserved.

17. Ploschner, M., Cizmar, T., Mazilu, M., Di Falco, A. & Dholakia, K. Bidirectional optical sorting of gold nanoparticles. *Nano Lett.* **12,** 1923–1927 (2012).
18. Tong, L., Miljkovic, V. D. & Kall, M. Alignment, rotation, and spinning of single plasmonic nanoparticles and nanowires using polarization dependent optical forces. *Nano Lett.* **10,** 268–273 (2010).
19. Geiselmann, M. *et al.* Three-dimensional optical manipulation of a single electron spin. *Nature Nanotech.* **8,** 175–179 (2013).
20. Reece, P. J. *et al.* Characterization of semiconductor nanowires using optical tweezers. *Nano Lett.* **11,** 2375–2381 (2011).
21. Chen, Y. F., Serey, X., Sarkar, R., Chen, P. & Erickson, D. Controlled photonic manipulation of proteins and other nanomaterials. *Nano Lett.* **12,** 1633–1637 (2012).
22. Pauzauskie, P. J. *et al.* Optical trapping and integration of semiconductor nanowire assemblies in water. *Nature Mater.* **5,** 97–101 (2006).
23. Ashkin, A. & Dziedzic, J. M. Optical trapping and manipulation of viruses and bacteria. *Science* **235,** 1517–1520 (1987).
24. Lauffer, M. A. & Stevens, C. L. Structure of the tobacco mosaic virus particle; polymerization of tobacco mosaic virus protein. *Adv. Virus Res.* **13,** 1–63 (1968).
25. Newman, J. & Swinney, H. L. Length and dipole moment of TMV by laser signal-averaging transient electric birefringence. *Biopolymers* **15,** 301–315 (1976).
26. Knipe, D. *et al. Fields Virology* (Lippincott, Williams & Wilkins, 2007).
27. Klein, J. S. & Bjorkman, P. J. Few and far between: how HIV may be evading antibody avidity. *PLoS Pathogens* **6,** e1000908 (2010).
28. Bendix, P. M. & Oddershede, L. B. Expanding the optical trapping range of lipid vesicles to the nanoscale. *Nano Lett.* **11,** 5431–5437 (2011).
29. Cheng, W., Hou, X. & Ye, F. Use of tapered amplifier diode laser for biological-friendly high-resolution optical trapping. *Opt. Lett.* **35,** 2988–2990 (2010).
30. Kim, J. H., Song, H., Austin, J. L. & Cheng, W. Optimized infectivity of the cell-free single-cycle human immunodeficiency viruses type 1 (HIV-1) and its restriction by host cells. *PLoS ONE* **8,** e67170 (2013).
31. McDonald, D. *et al.* Visualization of the intracellular behavior of HIV in living cells. *J. Cell Biol.* **159,** 441–452 (2002).
32. Schaeffer, E., Geleziunas, R. & Greene, W. C. Human immunodeficiency virus type 1 Nef functions at the level of virus entry by enhancing cytoplasmic delivery of virions. *J. Virol.* **75,** 2993–3000 (2001).
33. Accola, M. A., Ohagen, A. & Gottlinger, H. G. Isolation of human immunodeficiency virus type 1 cores: retention of Vpr in the absence of p6(gag). *J. Virol.* **74,** 6198–6202 (2000).
34. Hou, X. & Cheng, W. Single-molecule detection using continuous wave excitation of two-photon fluorescence. *Opt. Lett.* **36,** 3185–3187 (2011).
35. Hou, X. & Cheng, W. Detection of single fluorescent proteins inside eukaryotic cells using two-photon fluorescence. *Biomed. Opt. Express* **3,** 340–353 (2012).
36. Cheng, W., Arunajadai, S. G., Moffitt, J. R., Tinoco, I. Jr & Bustamante, C. Single-base pair unwinding and asynchronous RNA release by the hepatitis C virus NS3 helicase. *Science* **333,** 1746–1749 (2011).
37. Briggs, J. A. G., Wilk, T., Welker, R., Krausslich, H. G. & Fuller, S. D. Structural organization of authentic, mature HIV-1 virions and cores. *EMBO J.* **22,** 1707–1715 (2003).
38. Tolic-Norrelykke, S. F. *et al.* Calibration of optical tweezers with positional detection in the back focal plane. *Rev. Sci. Instrum.* **77,** 103101 (2006).
39. Burton, D. R. *et al.* Efficient neutralization of primary isolates of HIV-1 by a recombinant human monoclonal antibody. *Science* **266,** 1024–1027 (1994).
40. Kwong, P. D. *et al.* Structure of an HIV gp120 envelope glycoprotein in complex with the CD4 receptor and a neutralizing human antibody. *Nature* **393,** 648–659 (1998).
41. Liu, J., Bartesaghi, A., Borgnia, M. J., Sapiro, G. & Subramaniam, S. Molecular architecture of native HIV-1 gp120 trimers. *Nature* **455,** 109–113 (2008).
42. Chertova, E. *et al.* Envelope glycoprotein incorporation, not shedding of surface envelope glycoprotein (gp120/SU), is the primary determinant of SU content of purified human immunodeficiency virus type 1 and simian immunodeficiency virus. *J. Virol.* **76,** 5315–5325 (2002).
43. Zhu, P. *et al.* Distribution and three-dimensional structure of AIDS virus envelope spikes. *Nature* **441,** 847–852 (2006).
44. Gittes, F. & Schmidt, C. F. Interference model for back-focal-plane displacement detection in optical tweezers. *Opt. Lett.* **23,** 7–9 (1998).
45. Klasse, P. J. The molecular basis of HIV entry. *Cell Microbiol.* **14,** 1183–1192 (2012).
46. Parrish, N. F. *et al.* Phenotypic properties of transmitted founder HIV-1. *Proc. Natl Acad. Sci. USA* **110,** 6626–6633 (2013).
47. Berger, E. A. *et al.* A new classification for HIV-1. *Nature* **391,** 240 (1998).
48. Checkley, M. A., Luttge, B. G. & Freed, E. O. HIV-1 envelope glycoprotein biosynthesis, trafficking, and incorporation. *J. Mol. Biol.* **410,** 582–608 (2011).
49. Johnson, M. C. Mechanisms for Env glycoprotein acquisition by retroviruses. *AIDS Res. Hum. Retrovir.* **27,** 239–247 (2011).
50. Sundquist, W. I. & Krausslich, H. G. HIV-1 assembly, budding, and maturation. *Cold Spring Harb. Perspect. Med.* **2,** a006924 (2012).
51. Muranyi, W., Malkusch, S., Muller, B., Heilemann, M. & Krausslich, H. G. Super-resolution microscopy reveals specific recruitment of HIV-1 envelope proteins to viral assembly sites dependent on the envelope C-terminal tail. *PLoS Pathogens* **9,** e1003198 (2013).
52. Arunajadai, S. G. & Cheng, W. Step detection in single-molecule real time trajectories embedded in correlated noise. *PLoS ONE* **8,** e59279 (2013).

Acknowledgements

This work was supported by a National Institutes of Health (NIH) Director's New Innovator Award (1DP2OD008693-01, to W.C.), a National Science Foundation CAREER Award (CHE1149670, to W.C.) and also in part by a research grant from the March of Dimes Foundation (5-FY10-490, to W.C.). The authors thank A. Ono and A. Telesnitsky for discussions and Cheng Lab members, especially M. DeSantis, for critical reading of the manuscript. The MATLAB code for analysis of transmission electron microscopy images of polystyrene beads was provided by M. DeSantis. The following reagents were obtained through the AIDS Research and Reference Reagent Program, Division of AIDS, National Institute of Allergy and Infectious Diseases (NIAID), NIH: pNL4-3 from M. Martin; pNL4-3.Luc.R-E- from N. Landau; pEGFP–Vpr from W. C. Greene; TZM-bl cells from J. C. Kappes, X. Wu and Tranzyme Inc; b12 antibody from D. Burton and C. Barbas.

Author contributions

W.C. conceived and directed the project. H.S. and J.H.K. prepared experimental materials. Y.P., H.S., J.H.K., X.H. and W.C. conducted the experiments. Y.P., H.S., J.H.K., X.H. and W.C. performed the analysis. Y.P. and W.C. wrote the paper.

Additional information

Supplementary information is available in the online version of the paper. Reprints and permissions information is available online at www.nature.com/reprints. Correspondence and requests for materials should be addressed to W.C.

Competing financial interests

The authors declare no competing financial interests.

© 2014 Macmillan Publishers Limited. All rights reserved.